Electrochimica Acta 59 (2012) 329–335

Contents lists available at SciVerse ScienceDirect

Electrochimica Acta

journal homepage: www.elsevier.com/locate/electacta

Electrochemical reduction of oxygen on palladium nanocubes in acid and alkaline solutions

H. Erikson[a], A. Sarapuu[a], N. Alexeyeva[a,1], K. Tammeveski[a,*,1], J. Solla-Gullón[b,1], J.M. Feliu[b,1]

[a] Institute of Chemistry, University of Tartu, Ravila 14a, 50411 Tartu, Estonia
[b] Instituto de Electroquímica, Universidad de Alicante, Apartado 99, 03080 Alicante, Spain

ARTICLE INFO

Article history:
Received 24 August 2011
Received in revised form 20 October 2011
Accepted 24 October 2011
Available online 3 November 2011

Keywords:
Oxygen reduction
Palladium nanocubes
Palladium nanoparticles
Pd-based catalysts
Electrocatalysis

ABSTRACT

The electrocatalytic properties of cubic palladium nanoparticles towards the electrochemical reduction of oxygen were studied in acid and alkaline solutions and compared with those of spherical nanoparticles and bulk Pd. The synthesised Pd nanoparticles were characterised by transmission electron microscopy (TEM) and X-ray diffraction (XRD). Electrooxidation of pre-adsorbed CO was employed for cleaning the palladium catalyst surface. Oxygen reduction was studied using the rotating disk electrode (RDE) method and enhanced electrocatalytic activity of Pd nanocubes was revealed both in acid and alkaline solutions, which was attributed to the prevalence of Pd(1 0 0) facets. The mechanism of oxygen reduction on Pd nanoparticles was similar to that on bulk Pd, the first electron transfer being the rate-limiting step, and the reaction predominantly followed a four-electron pathway in both solutions.

1. Introduction

Nanostructured palladium catalysts have received much attention in recent years as rather active catalysts for the electrochemical reduction of oxygen [1,2]. Pd has properties similar to those of platinum and the mechanism of O_2 reduction in both acid and alkaline solutions is the same on these metals [3,4]. As compared to Pt, Pd is more abundant on the Earth and considerably cheaper [2], but the activity of pure Pd towards O_2 reduction is lower and Pd is less stable in acid media [1]. Bimetallic Pd-based catalysts, such as alloys and core–shell particles with non-noble metals (Co, Fe, etc.), have been shown to possess higher electrocatalytic activity for oxygen reduction than pure Pd [1,2]. A further advantage of Pd and its alloys is their good selectivity for oxygen reduction reaction (ORR) in the presence of alcohols, which makes them attractive catalysts for direct alcohol fuel cells [2].

There are several studies of oxygen reduction on nanostructured Pd catalysts in acid media [5–19]. The activity of Pd/C catalysts is generally considerably lower than that of Pt/C [8,9]. However, very high catalytic activity has been observed for Pd nanorods prepared by electrodeposition [10]. For vacuum-evaporated thin Pd films, the specific activity of O_2 reduction was similar to that of bulk Pd and slightly decreased with decreasing the film thickness in H_2SO_4 solution [11,12], but it was rather constant in $HClO_4$ [11]. Improved electrocatalytic properties for O_2 reduction have been observed on Pd nanoparticles (PdNPs) supported on carbon nanotubes [13–17]. For Pd/C catalysts, the activity can also be influenced by pre-treatment of the carbon support [18].

As on platinum, oxygen reduction on Pd is a structure-sensitive reaction [1]. It has been demonstrated that in $HClO_4$ solution, the ORR activity on Pd single crystals increases in the order of Pd(1 1 0) < Pd(1 1 1) < Pd(1 0 0) [20]. In contradiction to that, high catalytic activity of Pd nanorods as compared to spherical Pd nanoparticles has been attributed to the prevalence of Pd(1 1 0) facets [10]. Very recently, the oxygen reduction studies on Pd nanocubes with a preferential (1 0 0) surface orientation have been published [6,7]. The specific activity of cubic Pd particles was comparable to that of Pt, but the activity of Pd octahedra, however, was 10 times lower [6]. The higher ORR activity of Pd nanocubes was attributed to the lower coverage of chemisorbed OH, which in turn offers more available reaction sites [6], or, in H_2SO_4 solution, to the structure-dependent adsorption of (bi)sulphate ions [7]. In contrast, studies of the ORR on stepped surfaces of *n*(1 1 1)–(1 0 0) series of Pd in $HClO_4$ revealed that the activity increases with increasing the terrace atom density, although the oxide coverage also increases. It has been proposed that on Pd, the active sites for the ORR are the terraces [21].

In alkaline solutions, Pd catalysts have shown remarkably high activity and good stability and are therefore considered as promising electrocatalysts for alkaline fuel cells [19,22–29]. In some cases, activities comparable to that of Pt [23] or even higher [25,28] have

* Corresponding author. Tel.: +372 7375168; fax: +372 7375181.
E-mail addresses: kaido@chem.ut.ee, kaido.tammeveski@ut.ee (K. Tammeveski).
[1] ISE member.

0013-4686/$ – see front matter © 2011 Elsevier Ltd. All rights reserved.
doi:10.1016/j.electacta.2011.10.074

been observed. The specific activity of the Pd/C catalysts depends on the Pd particle size, decreasing by a factor of about three with decreasing particle size from 16.7 to 3 nm [24]. However, graphene-supported Pd nanoparticles with a mean diameter of only 1.8 nm showed significantly high catalytic activity for the ORR [28].

The aim of this study was to synthesise cubic Pd nanoparticles and to compare their electrocatalytic activity towards oxygen reduction with that of spherical Pd nanoparticles and bulk Pd in acidic as well as in alkaline solutions.

2. Experimental

2.1. Synthesis and characterisation of Pd nanoparticles

Pd nanocubes were synthesised using a previously described methodology [30] in which H_2PdCl_4 solution was reduced with ascorbic acid in the presence of cetyltrimethylammonium bromide (CTAB) at 95 °C. The sample was twice centrifugated and redispersed in water and the PdNPs were then cleaned with strong basic aqueous solution followed by washing 3–4 times in ultrapure water to finally achieve a water suspension. The synthesis of spherical Pd nanoparticles has been adapted from the citrate method usually employed for the synthesis of gold nanoparticles [31]. In brief, the metallic precursor (H_2PdCl_4) was reduced with ice-cold sodium borohydride in the presence of sodium citrate (which acts as stabiliser). Afterwards, solid NaOH was added to produce the precipitation of the nanoparticles. After complete precipitation, the nanoparticles were washed 3–4 times with ultrapure water.

The nanoparticles were characterised using a Transmission Electron Microscope (TEM) (JEM-2010, JEOL) working at 200 kV. The samples for TEM analysis were obtained by placing a droplet of the PdNPs suspension onto a formvar/carbon coated copper grid and allowing the solvent to evaporate in air at room temperature. X-ray diffractograms were recorded in a Bruker D8 advance diffractometer, using Cu Kα radiation ($\lambda = 0.15418$ nm) operated at 40 kV and 40 mA. Spectra were recorded between 30° and 90° (2θ) with a step of 0.1° and a time per step of 30 seconds. The PdNP samples for XRD analysis were prepared by evaporating a drop of nanoparticle suspension on a Si substrate.

2.2. Electrochemical measurements

Glassy carbon (GC) and bulk polycrystalline palladium electrodes were prepared by mounting GC (GC-20SS, Tokai Carbon) and Pd (99.95%, Alfa Aesar) disks into Teflon holders. The geometric area of the electrodes (A) was 0.2 cm^2. The surface of the GC electrodes was polished to a mirror finish with 1.0 and 0.3 μm alumina slurries (Buehler); bulk Pd electrodes were finished by polishing with a 0.05 μm alumina slurry. After polishing, the electrodes were ultrasonically cleaned in Milli-Q (Millipore, Inc.) water for 5 min.

An aliquot of the suspension of PdNPs in water was pipetted onto a polished GC substrate and the solvent was allowed to evaporate in air. In this work 4–5 electrodes were tested in each electrolyte. The GC electrode surface was freshly modified with PdNPs before electrochemical testing. Oxygen reduction was studied using the rotating disk electrode (RDE) technique. The solutions were prepared from 96% H_2SO_4 (Suprapur, Merck) or from KOH pellets (pro analysi, Merck) and Milli-Q water and were saturated with pure O_2 (99.999%, AGA) or deaerated with Ar gas (99.999%, AGA). A reversible hydrogen electrode (RHE) connected to the cell through a Luggin capillary was employed as a reference and all the potentials are referred to this electrode. A Pt wire served as a counter electrode and the counter electrode compartment of the three-electrode cell was separated from the main cell compartment by a glass frit. Potential was applied with an Autolab potentiostat/galvanostat PGSTAT30 (Eco Chemie B.V., The Netherlands). An EDI101 rotator and a CTV101 speed control unit (Radiometer, Copenhagen) were used for the RDE experiments. All experiments were carried out at room temperature (23 ± 1 °C).

Prior to the O_2 reduction measurements, the electrodes were electrochemically pre-treated in Ar-saturated 0.05 M H_2SO_4 or 0.1 M KOH solution by scanning the potential between 0.1 and 0.7 V. To clean the Pd surface, carbon monoxide (AGA) was adsorbed onto the Pd catalyst by bubbling CO through the electrolyte at 0.1 V until complete blockage of the surface, which was monitored by cycling the electrode between 0.1 and 0.35 V [32]. After that, CO was removed from the solution by bubbling argon for 45 min. Finally, CO was oxidatively stripped off from the surface by scanning the potential up to 1.0 V and the voltammogram corresponding to the CO-free surface was again recorded. After that the electrode was immediately transferred into an O_2-saturated solution in another cell in order to avoid surface contamination in air. For O_2 reduction measurements, the potential was scanned between 0.1 and 1 V at 10 mV s^{-1}.

3. Results and discussion

3.1. Surface characterisation of Pd nanoparticles

The TEM micrographs for cubic and spherical PdNPs synthesised are presented in Fig. 1. Fig. 1a shows the presence of a high percentage of Pd nanocubes, for which the (1 0 0) preferential surface structure is expected. In contrast, Fig. 1b shows quasi-spherical Pd particles which can be considered as representative of polyoriented, nonspecifically structured nanoparticles. The particle size determined from the TEM images was 26.9 ± 3.9 and 2.8 ± 0.4 nm for cubic and spherical PdNPs, respectively.

Fig. 2 shows the XRD patterns of the ~27 nm Pd nanocubes and ~3 nm Pd spheres. All the diffraction peaks can be well-indexed to face-centered cubic (fcc) palladium metal. Remarkably, the XRD pattern of Pd nanocubes shows an abnormally intense (2 0 0) peak, which is not observed for the Pd spheres, suggesting that most of the Pd nanocubes are preferentially oriented with their (1 0 0) facets parallel to the substrate. This feature has been previously observed with ~50–70 nm Pd nanocubes [30,33,34]. However, this (2 0 0) abnormally intense peak was not observed for 6–7 nm Pd nanocubes [6] which could suggest a "size effect". Nevertheless, ~60 [35] and ~24 nm Pd nanocubes [36] also showed the absence of this (2 0 0) abnormally intense peak. Additional experiments are required to clarify these discrepancies.

3.2. Cyclic voltammetry (CV) and CO stripping

In order to clean the surface of PdNPs without altering their initial morphology, residual impurities on the surface were displaced by adsorption of CO, followed by its oxidation [32]. Typical CO stripping voltammograms are presented in Fig. 3. In acid solution, a well-defined stripping peak of adsorbed CO was observed at 0.88 V for cubic PdNPs and at 0.91 V for spherical PdNPs. The second anodic peak at 0.94 V can be attributed to the surface oxidation on Pd(1 0 0) terraces. This characteristic signal has been well-studied in Pd(S) – [n(1 0 0) × (1 1 1)] [37] and Pd(S) – [n(1 0 0) × (1 1 0)] [38] electrodes and its charge has been reported to exclusively depend on the terrace atom density without contributions from step sites. The cathodic peak at ca 0.77 V corresponds to the reduction of Pd surface oxides. The CV response of PdNPs recorded after CO stripping (inset of Fig. 3a) showed improved definition and symmetry of the CV peaks as a result of increased cleanliness of the surface. The voltammetric profile of the cubic PdNPs resembles that characteristic of a Pd(1 0 0) single crystal and shows well-defined peaks

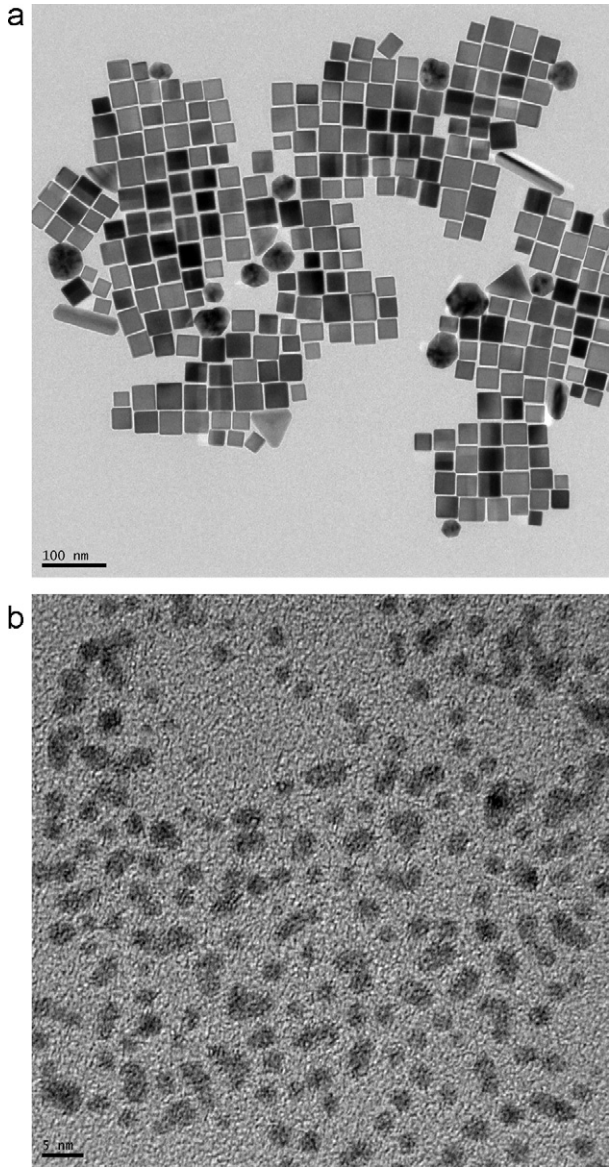

Fig. 1. TEM images of Pd catalysts: (a) cubic PdNPs and (b) spherical PdNPs.

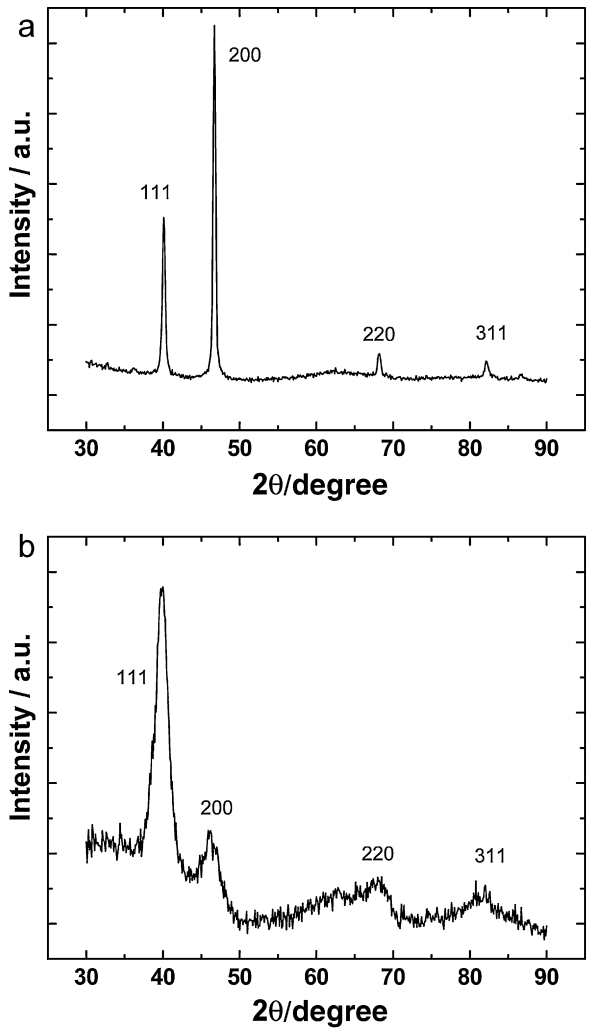

Fig. 2. XRD patterns of Pd catalysts: (a) cubic PdNPs and (b) spherical PdNPs.

at 0.35 and 0.22 V [37,38]. In alkaline solution (Fig. 3b) sharp CO stripping peaks appear at the potentials of 0.72 and 0.75 V for Pd nanocubes and spherical Pd nanoparticles, respectively. The peaks of hydrogen adsorption and desorption on CVs recorded after CO stripping are not as well-defined as in acid solution, but the peak characteristic to Pd(1 0 0) terraces can be observed at ca 0.55 V [39].

After the O_2 reduction measurements, the CV curves were again recorded in Ar-saturated 0.05 M H_2SO_4 or 0.1 M KOH by extending the anodic potential to 1.4 V (Fig. 4). The anodic peaks at $E > 0.7$ V and the cathodic peaks at ca 0.65–0.7 V correspond to the formation of Pd surface oxides and to their reduction, respectively. For cubic PdNPs in alkaline solution (Fig. 4b), characteristic peaks of hydrogen desorption and oxide formation at Pd(1 0 0) terraces are in evidence at the potentials of 0.58 and 0.87 V, respectively [39]. By integrating the charge under the cathodic peak, the real electroactive area (A_r) of Pd catalysts was estimated, assuming the value of 424 μC cm^{-2} as the charge density for the reduction of a monolayer of PdO [40]. For comparison, the real surface area of PdNPs was also determined from the H_{upd} desorption peaks on the CV curves registered in Ar-saturated 0.05 M H_2SO_4 (using the charge density of 212 μC cm^{-2}) [41] and the A_r values obtained by these two methods were in a good agreement with each other.

3.3. Oxygen reduction in acidic media

The electroreduction of O_2 on Pd nanoparticles and bulk Pd was studied in O_2-saturated 0.05 M H_2SO_4 solution using the RDE method. Fig. 5 shows the representative polarisation curves of O_2 reduction on cubic PdNPs at various rotation rates; the background current registered in O_2-free solution has been subtracted from these data and only the anodic sweeps are presented and subjected to further analysis. Similar single-wave polarisation curves were also observed for spherical PdNPs and bulk Pd. A comparison of the O_2 reduction data at a single electrode rotation rate is presented in Fig. 6.

The RDE data were analysed using the Koutecky–Levich (K–L) equation [42]:

$$\frac{1}{j} = \frac{1}{j_k} + \frac{1}{j_d} = -\frac{1}{nFkC^b_{O_2}} - \frac{1}{0.62nFD^{2/3}_{O_2}\nu^{-1/6}C^b_{O_2}\omega^{1/2}} \quad (1)$$

where j is the measured current density, j_k and j_d are the kinetic and diffusion-limited current densities, respectively, n is the number of electrons transferred per O_2 molecule, k is the rate constant for O_2 reduction, F is the Faraday constant (96 485 C mol^{-1}), ω is the electrode rotation rate, $C^b_{O_2}$ is the concentration of oxygen in the bulk

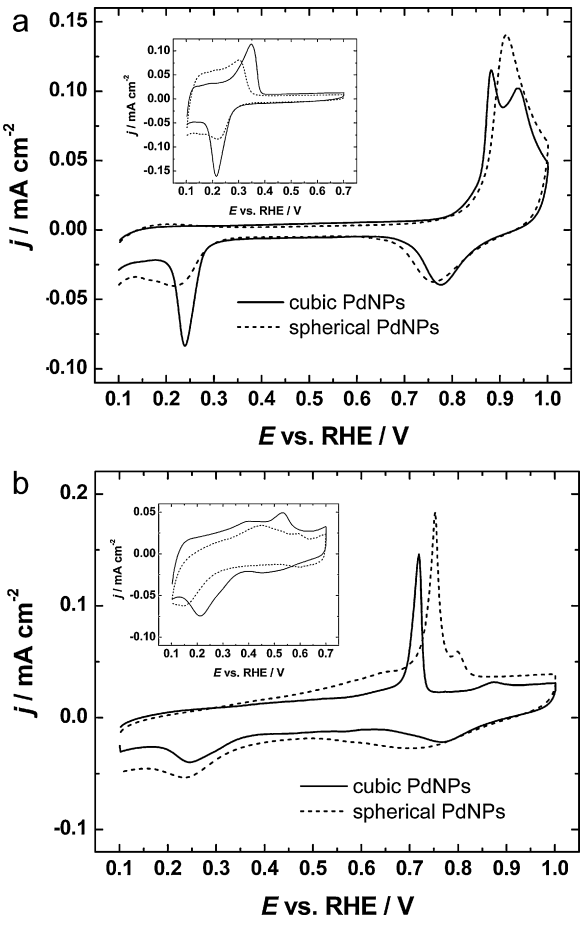

Fig. 3. Oxidation of pre-adsorbed CO on PdNP modified GC electrodes in Ar-saturated 0.05 M H_2SO_4 (a) and 0.1 M KOH (b). $\nu = 20\,mV\,s^{-1}$. *Insets*: CV curves for PdNPs after CO stripping, $\nu = 50\,mV\,s^{-1}$. Current densities are normalised to the real surface area of Pd.

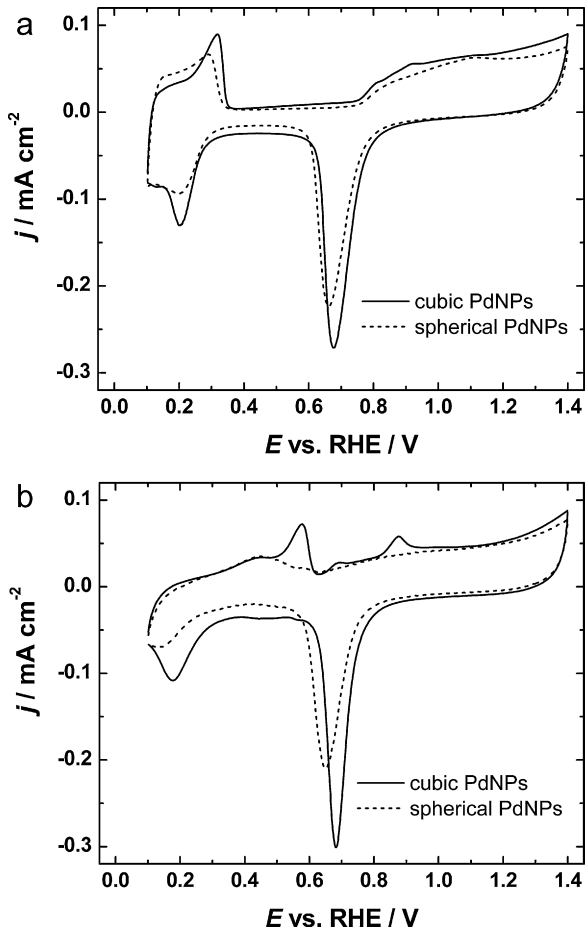

Fig. 4. Cyclic voltammograms for PdNP modified GC electrodes after O_2 reduction measurements in Ar-saturated 0.05 M H_2SO_4 (a) and 0.1 M KOH (b). $\nu = 50\,mV\,s^{-1}$. Current densities are normalised to the real surface area of Pd.

$(1.22 \times 10^{-6}\,mol\,cm^{-3})$ [43], D_{O_2} is the diffusion coefficient of oxygen $(1.93 \times 10^{-5}\,cm^2\,s^{-1})$ [43] and ν is the kinematic viscosity of the solution $(0.01\,cm^2\,s^{-1})$ [44]. The K–L plots were constructed (inset of Fig. 5) and the number of electrons transferred per O_2 molecule (n) was calculated from Eq. (1). On PdNPs, the value of n was close to four at negative potentials, which is in accordance with the earlier studies [5,7,11,12,19]. At more positive potentials, however, the n value decreased to about 3.5 at $E = 0.7$ V, indicating that H_2O_2 is produced to some extent. This may be due to the decreased activity of hydrogen peroxide reduction on Pd nanoparticles in H_2SO_4 solution [45]. On bulk Pd the $4e^-$ reduction proceeds in the whole range of potentials studied.

Comparison of the j–E curves of oxygen reduction on PdNPs and bulk Pd (Fig. 6) shows that the onset potential of O_2 reduction is about 60 mV more positive for Pd nanocubes than for spherical PdNPs and bulk Pd. This increased activity of O_2 reduction is most probably related to the morphological features of cubic PdNPs, specifically, to the predominance of Pd(1 0 0) surface sites. The ORR activity of Pd single crystals in $HClO_4$ has been shown to increase in the following order: Pd(1 1 0) < Pd(1 1 1) < Pd(1 0 0) [20]. In addition, in H_2SO_4 solution, the adsorption of (bi)sulphate ions may also have an influence to the O_2 reduction activity. It is well known that on the surface of platinum, (bi)sulphate ions show the strongest specific adsorption on Pt(1 1 1) sites, thereby blocking the O_2 adsorption centers and also having a negative electronic effect on the ORR kinetics [46]. On Pd the adsorption of anions is even stronger than on Pt [1] and therefore it is also expected that the presence of Pd(1 1 1) sites decreases the O_2 reduction activity on polyoriented PdNPs and bulk Pd as compared to cubic PdNPs that have mostly (1 0 0) facets on the surface. This is also supported by an IRAS study, which shows that the coverage of (bi)sulphate anions on Pd(1 0 0) is lower than that of Pd(111) [47].

It is evident from Fig. 6 that for PdNPs (both cubic and spherical) the oxygen reduction current does not increase as sharply as for bulk Pd and the kinetic region is wider. We suggest that this is due to

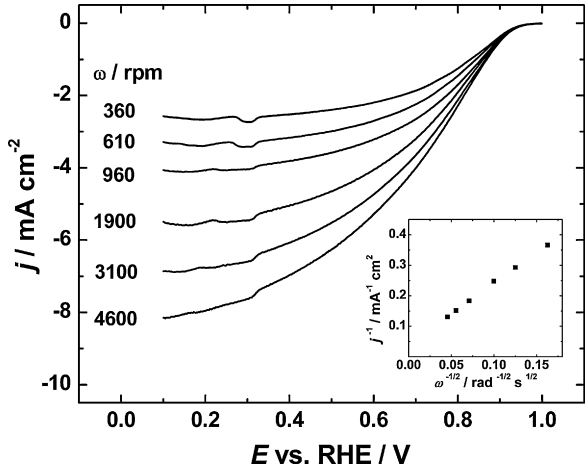

Fig. 5. RDE voltammetry curves for O_2 reduction on cubic PdNP modified GC electrodes in O_2-saturated 0.05 M H_2SO_4. $\nu = 10\,mV\,s^{-1}$. *Inset*: Koutecky-Levich plot for O_2 reduction at 0.3 V.

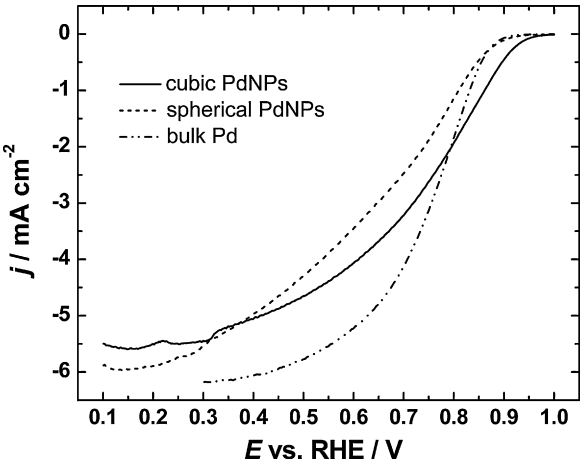

Fig. 6. A comparison of RDE voltammetry curves on PdNP modified GC electrodes (A_r = 0.56 cm^2 and A_r = 0.53 cm^2 for cubic and spherical PdNPs, respectively) and bulk Pd (A_r = 0.57 cm^2) in O_2-saturated 0.05 M H_2SO_4. ω = 1900 rpm, ν = 10 mV s^{-1}.

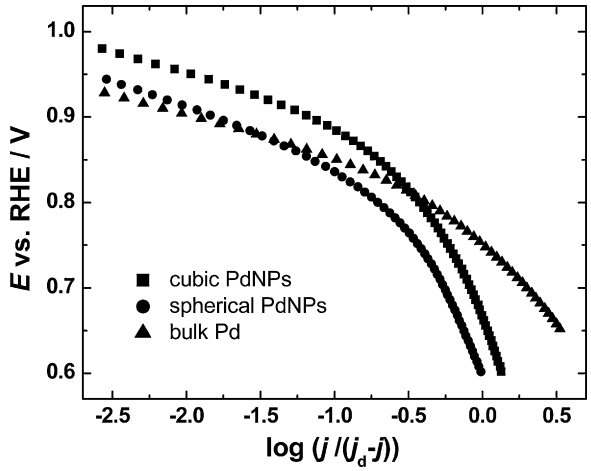

Fig. 7. Mass-transfer corrected Tafel plots for oxygen reduction on PdNP modified GC electrodes and bulk Pd in 0.05 M H_2SO_4. ω = 1900 rpm.

the uneven coating of the electrode substrate with PdNPs [48]. Bulk Pd shows a higher reduction current at E < 0.8 V, but this potential is already close to the half-wave potential of oxygen reduction and therefore not relevant from the electrode kinetics point of view. Based on these considerations, it appears that 0.85 V is the most appropriate potential for the determination of the intrinsic electrocatalytic activity of Pd catalysts for oxygen reduction in H_2SO_4 solution.

The specific activities (SA) of Pd catalysts at 0.85 V were calculated:

$$\mathrm{SA} = \frac{I_k}{A_r} \quad (2)$$

where I_k is the kinetic current at a given potential and A_r is the real electroactive area of palladium. The SA value for Pd nanocubes appeared to be considerably higher than these of spherical Pd nanoparticles and bulk Pd (Table 1). This is in accordance with the recent studies on Pd nanocubes in acid solutions, where about three times higher SA value was obtained for Pd nanocubes deposited onto Au electrode in 0.5 M H_2SO_4 solution than for spherical Pd nanoparticles [7]. In addition, an activity increase of Pd nanocubes of about 10 and 6 times over Pd/C octahedra and a commercial Pd/C catalyst, respectively, has been recently found in $HClO_4$ solution [6]. Similarly, for Pt nanocubes with preferential (1 0 0) surface orientation, an enhancement in oxygen reduction as compared to polycrystalline Pt nanoparticles has been observed [49,50]. On spherical PdNPs, the ORR activity is slightly lower than that on bulk Pd, which is in accordance with the results obtained on polyoriented nanostructured Pd electrodes, where the SA values were somewhat lower than that of bulk Pd [12]. This can be attributed to the influence of Pd particle size and/or morphology.

On the basis of the RDE data at 1900 rpm (Fig. 6) the mass-transfer corrected Tafel plots were constructed (Fig. 7) and the Tafel slopes were determined (Table 1). In the low current density region, the values of the Tafel slope for Pd nanocatalysts were slightly higher than −60 mV, which is the typical value for bulk polycrystalline Pd [3] and nanostructured Pd catalysts [11,12,18,51]. At higher current densities, the Tafel slope values near to −120 mV have been observed for bulk Pd [3], Pd/C catalysts [18] and thin Pd films [11,12], whereas a constantly changing Tafel slope has been reported in Ref. [51]. The Tafel slope values of −60 and −120 mV are also characteristic for O_2 reduction on Pt catalysts [52]. A change in the slope has been attributed to the change from Temkin to Langmuir conditions for the adsorption of reaction intermediates, but the transfer of the first electron to O_2 is the rate determining step in both regions [52]. The Tafel slope values obtained in this work suggest that the reaction mechanism on Pd nanoparticles is the same as on bulk Pd and Pt.

Table 1
Kinetic parameters for oxygen reduction on PdNPs and bulk Pd in 0.05 M H_2SO_4. ω = 1900 rpm.

Catalyst	Tafel slope (mV) I region[a]	Tafel slope (mV) II region[a]	SA at 0.85 V (mA cm^{-2})
Cubic PdNPs	−67 ± 11	−151 ± 27	0.35 ± 0.09
Spherical PdNPs	−81 ± 12	−156 ± 20	0.15 ± 0.02
Bulk Pd	−61 ± 1	−126 ± 2	0.20 ± 0.02

[a] Region I corresponds to low current densities and Region II to high current densities.

3.4. Oxygen reduction in alkaline media

For comparison purposes, the reduction of oxygen on PdNPs was studied also in alkaline solution. In Fig. 8, a series of RDE voltammetry curves of O_2 reduction on Pd nanocubes is shown. As compared to the results in acid, the electrocatalytic activity of Pd is higher in alkaline solution and a well-defined diffusion-limited current plateau is formed. Based on the RDE data, the K–L plots were constructed (inset of Fig. 8) and from Eq. (1), the value of $n \approx 4$ was

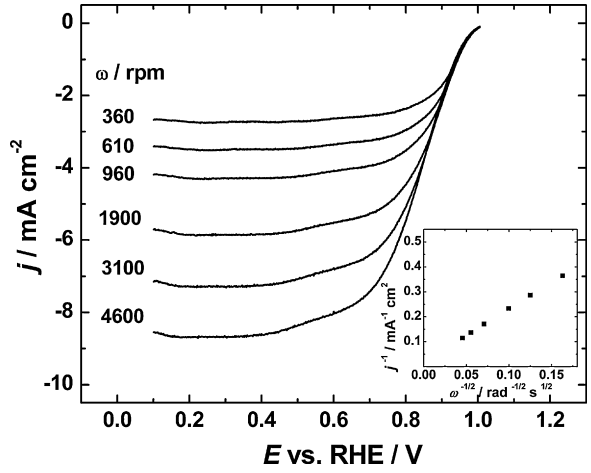

Fig. 8. RDE voltammetry curves for O_2 reduction on cubic PdNP modified GC electrodes in O_2-saturated 0.1 M KOH. ν = 10 mV s^{-1}. *Inset*: Koutecky–Levich plot for O_2 reduction at 0.3 V.

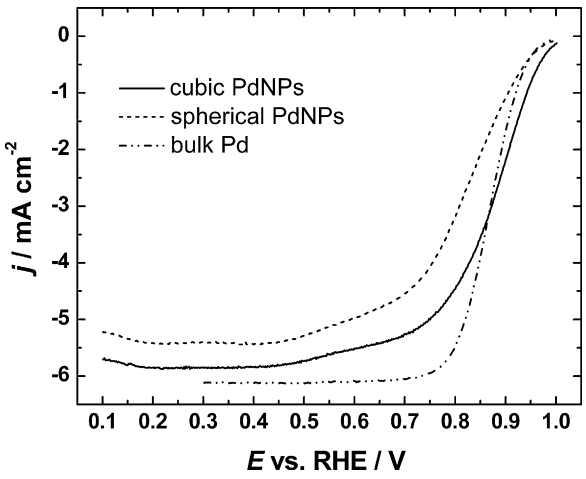

Fig. 9. A comparison of RDE voltammetry curves on PdNP modified GC electrodes (A_r = 0.64 cm^2 and A_r = 0.91 cm^2 for cubic and spherical PdNPs, respectively) and bulk Pd (A_r = 0.67 cm^2) in O_2-saturated 0.1 M KOH. ω = 1900 rpm, ν = 10 mV s^{-1}.

determined for cubic as well as spherical PdNPs and bulk Pd over the whole range of potentials, using the following values of diffusion coefficient and solubility of oxygen: $D_{O_2} = 1.9 \times 10^{-5}$ cm^2 s^{-1} and $C^b_{O_2} = 1.2 \times 10^{-6}$ mol cm^{-3} [53]. The 4e$^-$ reduction of O_2 in alkaline solutions has been also observed on Pd nanoparticles in earlier studies [24,25,28], however, it has been proposed that on Pt-group metals this reaction proceeds at least partly via peroxide intermediate [4].

In Fig. 9, the data at a single electrode rotation rate are compared for PdNPs and bulk Pd. The onset potential of O_2 reduction is the highest for Pd nanocubes and the sharpest current increase was observed for bulk Pd. The mass-transfer corrected Tafel plots were constructed from these data (Fig. 10) and the values of Tafel slope were determined (Table 2). At low current densities, Tafel slopes are similar for PdNPs and bulk Pd and slightly higher than −60 mV that is usually observed on Pd nanocatalysts [24,25,29]. For PdNPs, the slope value gradually increases at more negative potentials, up to about −180 mV. For bulk Pd, however, the slope is rather constant in the range of Tafel analysis, similarly to the results obtained by Vracar et al. in strongly alkaline solutions [3]. On Pt electrodes, two Tafel slope values (−60 and −120 mV) have been confirmed in many researches and it has been suggested that the ORR mechanism is the same on Pd [4].

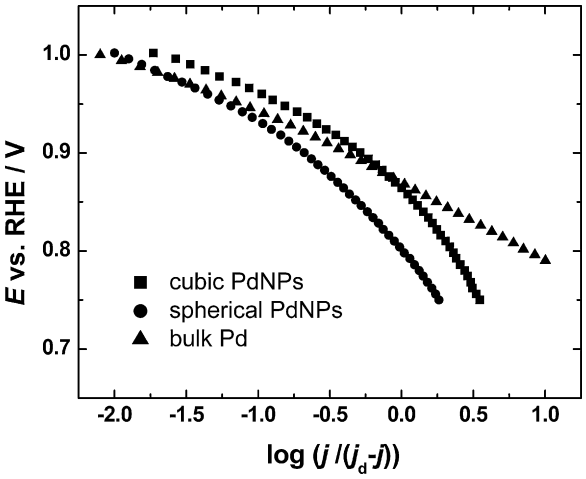

Fig. 10. Mass-transfer corrected Tafel plots for oxygen reduction on PdNP modified GC electrodes and bulk Pd in 0.1 M KOH. ω = 1900 rpm.

Table 2
Kinetic parameters for oxygen reduction on PdNPs and bulk Pd in 0.1 M KOH. ω = 1900 rpm.

Catalyst	Tafel slope (mV) I region[a]	Tafel slope (mV) II region[a]	SA at 0.95 V (mA cm^{-2})
Cubic PdNPs	−79 ± 3	−180 ± 26	0.28 ± 0.06
Spherical PdNPs	−77 ± 13	−181 ± 11	0.073 ± 0.005
Bulk Pd	−75 ± 3		0.13 ± 0.01

[a] Region I corresponds to low current densities and Region II to high current densities.

The values of the specific activities at 0.95 V calculated from Eq. (2) are given in Table 2. A rather positive potential was chosen to allow a better comparison with state-of-the-art cathode catalysts. Similarly to the results obtained in acid solution, the SA increases in the sequence: spherical PdNPs < bulk Pd < cubic PdNPs and it is most likely due to the morphological differences of PdNPs. To our knowledge, the ORR on Pd single crystals has not yet been systematically studied in alkaline solution, but the results in perchloric acid suggest that Pd(1 0 0) is the most active facet [20]. The lowest activity of spherical PdNPs may also be related to the particle size effect, as it has been shown that in alkaline solution the specific activity of Pd particles towards the ORR decreases by a factor of about 3 with decreasing the particle size from 16.7 to 3 nm [24]. This has been attributed to the stronger adsorption of OH on smaller particles that block the active reaction sites [24]; similar explanation has been given in case of Pt catalysts in alkaline solution [54–56]. The lowest OH coverage on Pd nanocubes has been also proposed as the reason of their high activity in $HClO_4$ solution [6]. However, it has been shown recently that in case of Pd single crystal electrodes in $HClO_4$, the oxide coverage is not relevant to the ORR and the activity depends only on the width of terraces, Pd(1 0 0) being the most active site [20,21]. In addition, for nanostructured Pd electrodes in 0.1 M KOH, no particle size dependence of the ORR was observed [12]. Therefore, it is most likely that the high activity of Pd nanocubes is due to the prevalence of Pd(1 0 0) surface sites, but it is not entirely clear at this stage of work, what is the reason of the high activity of Pd(1 0 0) in alkaline solutions.

4. Conclusions

The cubic palladium nanoparticles synthesised in this work showed enhanced electrocatalytic activity towards electroreduction of oxygen, as compared to spherical Pd nanoparticles or bulk Pd. This effect was observed in acidic as well as in alkaline solution and is most probably related to the predominance of the Pd(1 0 0) surface sites on Pd nanocubes. The four-electron reduction of oxygen to water was observed on Pd catalysts studied and the Tafel analysis revealed that the mechanism of O_2 reduction is the same on Pd nanoparticles as on bulk palladium or platinum in acidic solution. The shape-controlled synthesis of metal nanoparticles enables to design more active catalysts for O_2 reduction that have potential applications in low temperature fuel cells.

Acknowledgements

This research was supported by the Estonian Science Foundation (Grant No. 8380). Partial financial support by the CRDF-ETF grant (Project No. ESC2-2975-TR-09) is gratefully acknowledged. This work has been also financially supported by the MICINN of Spain through the project CTQ2010-16271 (FEDER).

References

[1] M. Shao, J. Power Sources 196 (2011) 2433.
[2] E. Antolini, Energy Environ. Sci. 2 (2009) 915.

[3] L.M. Vracar, D.B. Sepa, A. Damjanovic, J. Electrochem. Soc. 133 (1986) 1835.
[4] J.S. Spendelow, A. Wieckowski, Phys. Chem. Chem. Phys. 9 (2007) 2654.
[5] J.J. Salvador-Pascual, S. Citalan-Cigarroa, O. Solorza-Feria, J. Power Sources 172 (2007) 229.
[6] M.H. Shao, T.Y. Yu, J.H. Odell, M.S. Jin, Y.N. Xia, Chem. Commun. 47 (2011) 6566.
[7] H. Erikson, A. Sarapuu, K. Tammeveski, J. Solla-Gullon, J.M. Feliu, Electrochem. Commun. 13 (2011) 734.
[8] M.H. Shao, K. Sasaki, R.R. Adzic, J. Am. Chem. Soc. 128 (2006) 3526.
[9] J.H. Yang, J.Y. Lee, Q.B. Zhang, W.J. Zhou, Z.L. Liu, J. Electrochem. Soc. 155 (2008) B776.
[10] L. Xiao, L. Zhuang, Y. Liu, J.T. Lu, H.D. Abruna, J. Am. Chem. Soc. 131 (2009) 602.
[11] A. Sarapuu, A. Kasikov, N. Wong, C.A. Lucas, G. Sedghi, R.J. Nichols, K. Tammeveski, Electrochim. Acta 55 (2010) 6768.
[12] H. Erikson, A. Kasikov, C. Johans, K. Kontturi, K. Tammeveski, A. Sarapuu, J. Electroanal. Chem. 652 (2011) 1.
[13] S. Chakraborty, C.R. Raj, Carbon 48 (2010) 3242.
[14] J.S. Ye, Y.C. Bai, W.D. Zhang, Microchim. Acta 165 (2009) 361.
[15] Y.H. Lin, X.L. Cui, X.R. Ye, Electrochem. Commun. 7 (2005) 267.
[16] S. Takenaka, N. Susuki, H. Miyamoto, E. Tanabe, H. Matsune, M. Kishida, Chem. Commun. 46 (2010) 8950.
[17] S. Takenaka, N. Susuki, H. Miyamoto, E. Tanabe, H. Matsune, M. Kishida, J. Catal. 279 (2011) 381.
[18] S.M. Senthil Kumar, J. Soler Herrero, S. Irusta, K. Scott, J. Electroanal. Chem. 647 (2010) 211.
[19] N. Alexeyeva, A. Sarapuu, K. Tammeveski, F.J. Vidal-Iglesias, J. Solla-Gullon, J.M. Feliu, Electrochim. Acta 56 (2011) 6702.
[20] S. Kondo, M. Nakamura, N. Maki, N. Hoshi, J. Phys. Chem. C 113 (2009) 12625.
[21] A. Hitotsuyanagi, S. Kondo, M. Nakamura, N. Hoshi, J. Electroanal. Chem. 657 (2011) 123.
[22] Y.F. Yang, Y.H. Zhou, C.S. Cha, Electrochim. Acta 40 (1995) 2579.
[23] F.H.B. Lima, J. Zhang, M.H. Shao, K. Sasaki, M.B. Vukmirovic, E.A. Ticianelli, R.R. Adzic, J. Phys. Chem. C 111 (2007) 404.
[24] L. Jiang, A. Hsu, D. Chu, R. Chen, J. Electrochem. Soc. 156 (2009) B643.
[25] L. Jiang, A. Hsu, D. Chu, R. Chen, J. Electrochem. Soc. 156 (2009) B370.
[26] T.G. Nikiforova, Y.V. Kabeneva, O.A. Runova, Russ. J. Appl. Chem. 83 (2010) 1001.
[27] F.H.B. Lima, J. Zhang, M.H. Shao, K. Sasaki, M.B. Vukmirovic, E.A. Ticianelli, R.R. Adzic, J. Solid State Electrochem. 12 (2008) 399.
[28] M.H. Seo, S.M. Choi, H.J. Kim, W.B. Kim, Electrochem. Commun. 13 (2011) 182.
[29] M.H. Shao, K. Sasaki, P. Liu, R.R. Adzic, Z. Phys. Chem. 221 (2007) 1175.
[30] W.X. Niu, Z.Y. Li, L.H. Shi, X.Q. Liu, H.J. Li, S. Han, J. Chen, G.B. Xu, Cryst. Growth Des. 8 (2008) 4440.
[31] M.C. Daniel, D. Astruc, Chem. Rev. 104 (2004) 293.
[32] J. Solla-Gullon, V. Montiel, A. Aldaz, J. Clavilier, J. Electroanal. Chem. 491 (2000) 69.
[33] W.X. Niu, L. Zhang, G.B. Xu, ACS Nano 4 (2010) 1987.
[34] L. Zhang, W.X. Niu, G.B. Xu, Nanoscale 3 (2011) 678.
[35] F.R. Fan, A. Attia, U.K. Sur, J.B. Chen, Z.X. Xie, J.F. Li, B. Ren, Z.Q. Tian, Cryst. Growth Des. 9 (2009) 2335.
[36] Y.C. Yu, Y.X. Zhao, T. Huang, H.F. Liu, Mater. Res. Bull. 45 (2010) 159.
[37] N. Hoshi, K. Kagaya, Y. Hori, J. Electroanal. Chem. 485 (2000) 55.
[38] N. Hoshi, M. Kuroda, Y. Hori, J. Electroanal. Chem. 521 (2002) 155.
[39] N. Hoshi, M. Nakamura, N. Maki, S. Yamaguchi, A. Kitajima, J. Electroanal. Chem. 624 (2008) 134.
[40] M. Grden, M. Lukaszewski, G. Jerkiewicz, A. Czerwinski, Electrochim. Acta 53 (2008) 7583.
[41] R. Woods, in: A.J. Bard (Ed.), Electroanalytical Chemistry, vol. 9, Marcel Dekker, New York, 1976, p. 1.
[42] A.J. Bard, L.R. Faulkner, Electrochemical Methods, 2nd ed., Wiley, New York, 2001.
[43] R.R. Adzic, J. Wang, B.M. Ocko, Electrochim. Acta 40 (1995) 83.
[44] D.R. Lide (Ed.), CRC Handbook of Chemistry and Physics, CRC Press, Boca Raton, 2001.
[45] D.X. Cao, L.M. Sun, G.L. Wang, Y.Z. Lv, M.L. Zhang, J. Electroanal. Chem. 621 (2008) 31.
[46] J.X. Wang, N.M. Markovic, R.R. Adzic, J. Phys. Chem. B 108 (2004) 4127.
[47] N. Hoshi, M. Kuroda, O. Koga, Y. Hori, J. Phys. Chem. B 106 (2002) 9107.
[48] Y. Garsany, O.A. Baturina, K.E. Swider-Lyons, S.S. Kocha, Anal. Chem. 82 (2010) 6321.
[49] C. Wang, H. Daimon, Y. Lee, J. Kim, S. Sun, J. Am. Chem. Soc. 129 (2007) 6974.
[50] M. Inaba, M. Ando, A. Hatanaka, A. Nomoto, K. Matsuzawa, A. Tasaka, T. Kinumoto, Y. Iriyama, Z. Ogumi, Electrochim. Acta 52 (2006) 1632.
[51] G.F. Alvarez, M. Mamlouk, S.M. Senthil Kumar, K. Scott, J. Appl. Electrochem. 41 (2011) 925.
[52] M.R. Tarasevich, Elektrokhimiya 9 (1973) 599.
[53] R.E. Davis, G.L. Horvath, C.W. Tobias, Electrochim. Acta 12 (1967) 287.
[54] J. Perez, E.R. Gonzalez, E.A. Ticianelli, Electrochim. Acta 44 (1998) 1329.
[55] L. Genies, R. Faure, R. Durand, Electrochim. Acta 44 (1998) 1317.
[56] K. Tammeveski, T. Tenno, J. Claret, C. Ferrater, Electrochim. Acta 42 (1997) 893.